Electronic Supplementary Material (ESI) for Nanoscale

Supplementary Information

Self-supported efficient hydrogen evolution catalysts with a core-shell structure designed via phase separation

Zhibin Li[1], Ruoyu Wu[1], Yuren Wen,[2] Fu-Kuo Chiang[3], Xiong-Jun Liu[1,], Jing Wang[1], Rui Li[4], Hui Wang[1], Yuan Wu[1], Suihe Jiang[1], Xianzhen Wang[5], Zhao-Ping Lu[1,]**

[1]State Key Laboratory for Advanced Metals and Materials, University of Science and Technology Beijing, Beijing 100083, P. R. China

[2]School of Materials Science and Engineering, University of Science and Technology Beijing, Beijing 100083, P. R. China

[3]National Institute of Clean-and-Low-Carbon Energy, P.O. Box 001 Shenhua NICE, Beijing 102211, P. R. China

[4]Northwestern Polytechnical University, Xi'an 710072, P. R. China

[5]Institute for Advanced Materials and Technology, University of Science and Technology Beijing, Beijing 100083, P. R. China

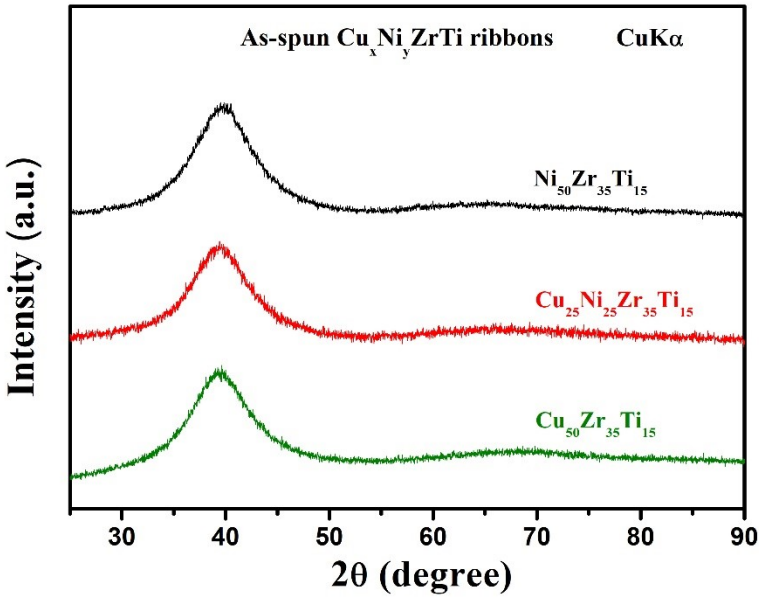

Figure S1. XRD patterns of the as-spun $Ni_xCu_{50-x}Zr_{35}Ti_{15}$ (x=0, 25, 50 at.%) MGs ribbons

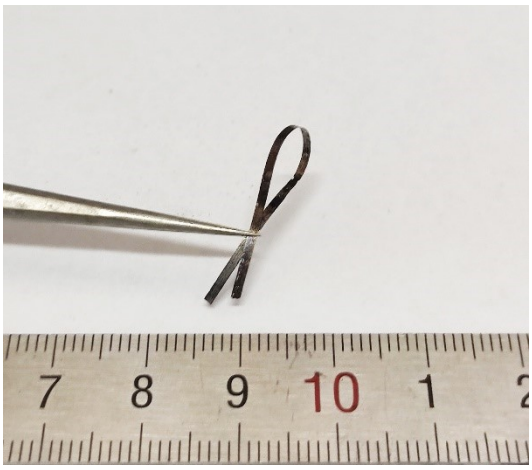

Figure S2. Optical image of the nanoporous Cu@(Ni/NiO) /glassy hybrid electrode

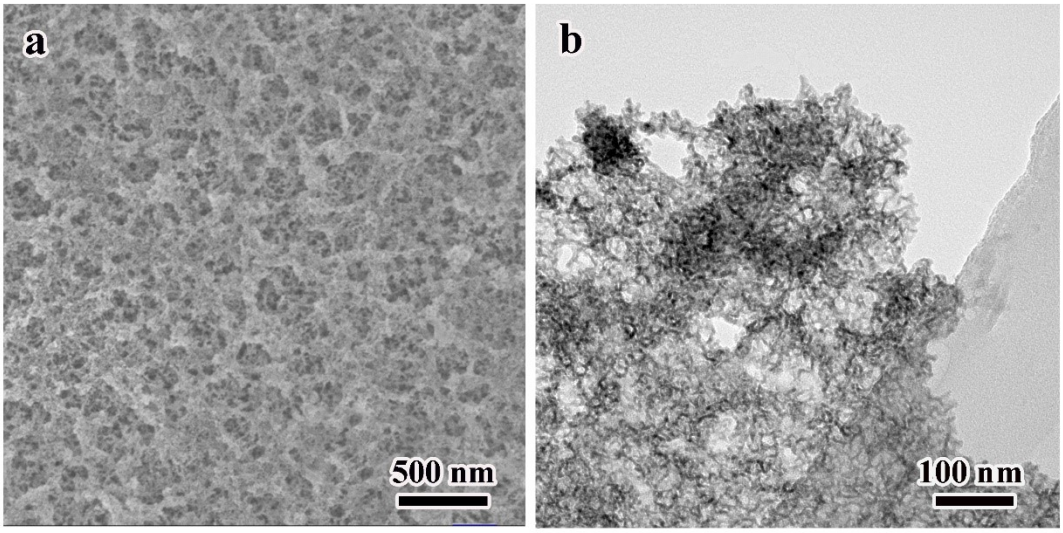

Figure S3. Surface morphology of the as-dealloyed $Ni_{50}Zr_{35}Ti_{15}$ ribbons for a constant dealloying time in the 0.1 mol/L HF aqueous solution at room temperature. a) SEM and b) TEM images

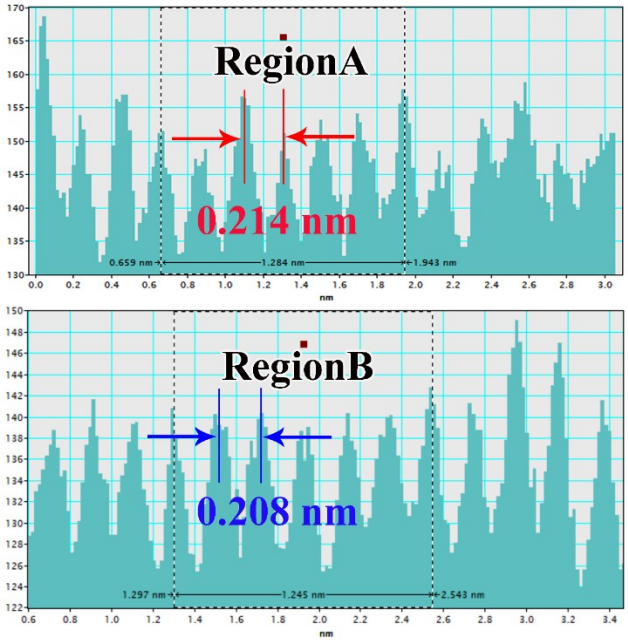

Figure S4. The line profiles of region A and B as marked in Fig. 2(b).

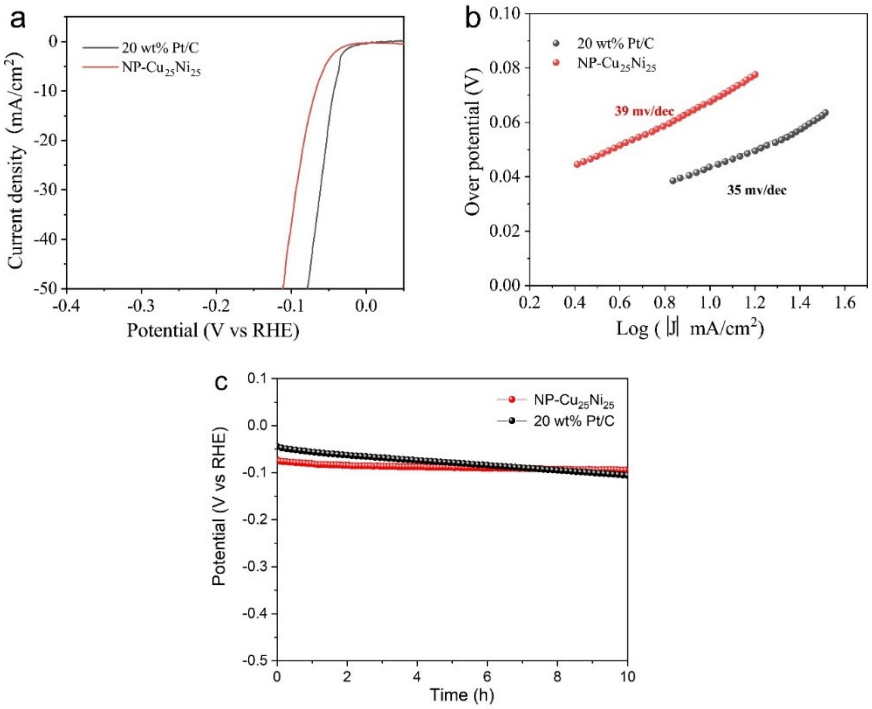

Figure S5. a) Polarization curves of the NP-$Cu_{25}Ni_{25}$ and the benchmark 20 wt % Pt/C electrocatalysts; b) Tafel slopes for the corresponding electrocatalysts. c. Stability comparison between commercial Pt/C and NP-$Cu_{25}Ni_{25}$ electrodes in 1 M KOH at a hydrogen evolution current of 10 mA cm^{-2}.

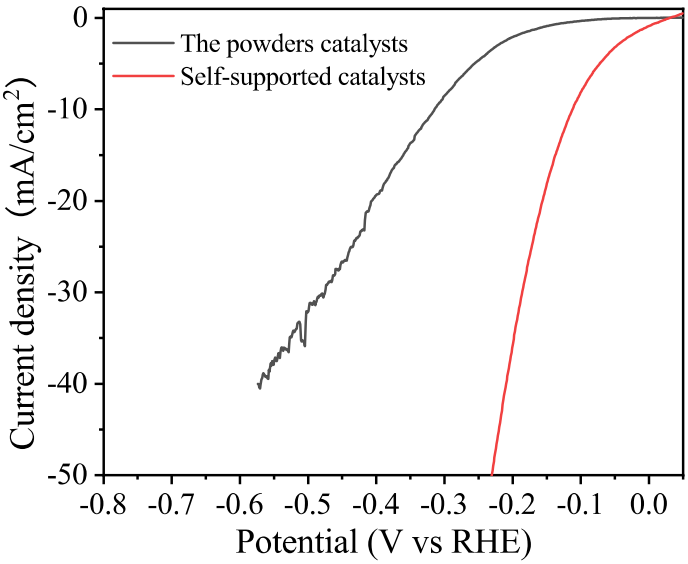

Figure S6. Polarization curves of the core-shell-structured Cu@(Ni/NiO) powder catalysts and self-supported core-shell-structured Cu@(Ni/NiO) catalysts, without iR-corrected.

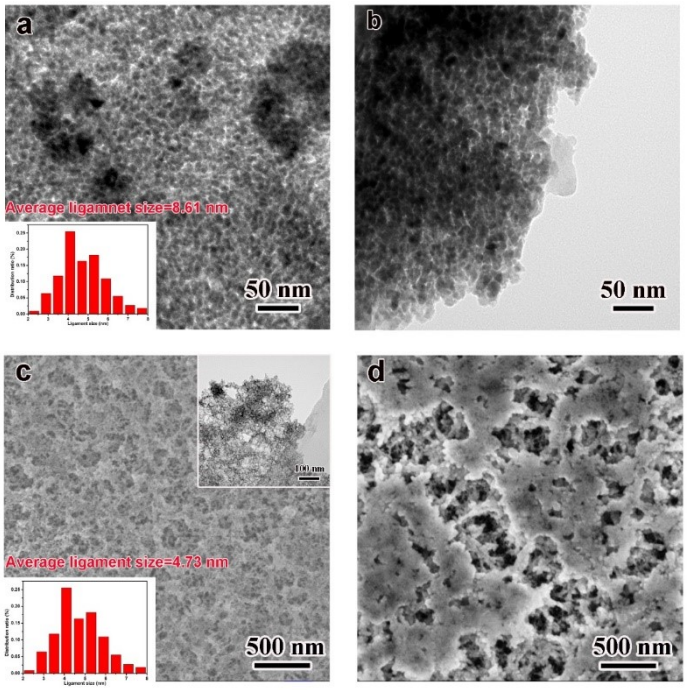

Figure S7. TEM images of the NP-$Cu_{25}Ni_{25}$ electrode before (a) and after 24 h HER stability test (b) Surface SEM images of the NP-Ni_{50} electrode before (c) and after 12 h HER stability test (d) The insets show the corresponding TEM image.

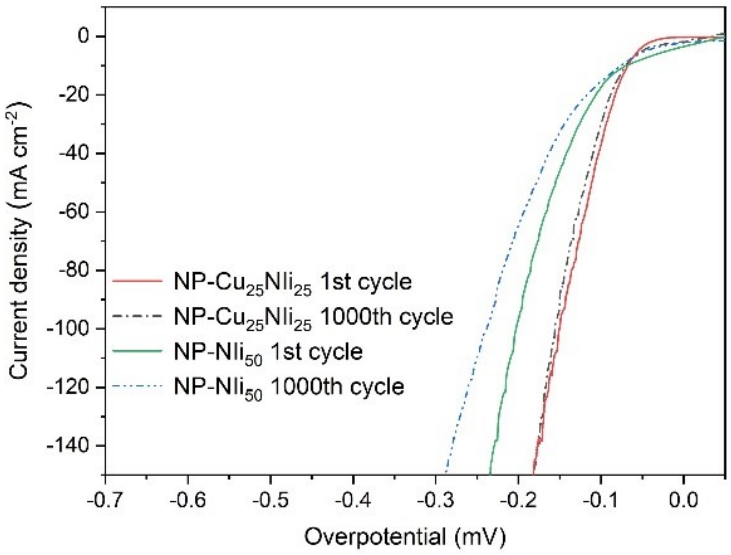

Figure S8. Polarization curves of the NP-$Cu_{25}Ni_{25}$ and NP-Ni_{50} electrodes before and after 1000 CV cycles.

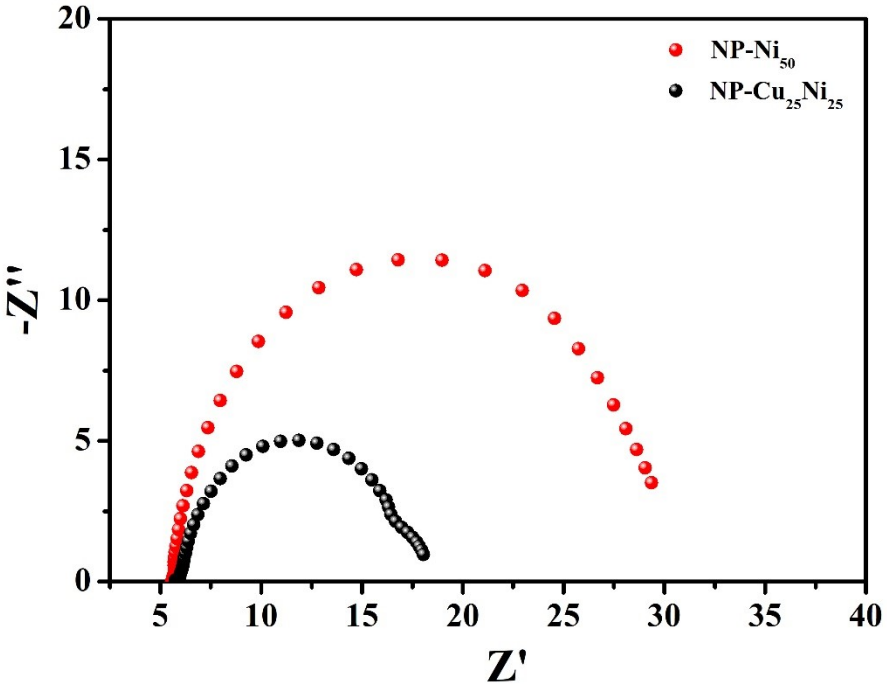

Figure S9. Nyquist plots of the NP-Ni_{50} and NP-$Ni_{25}Cu_{25}$.

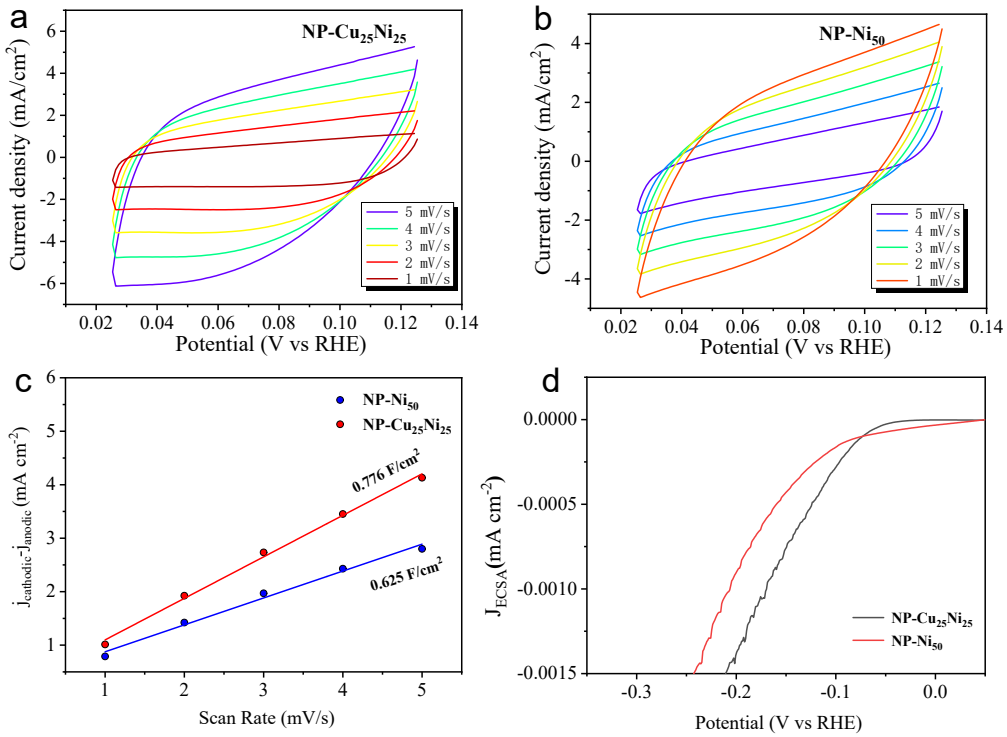

Figure S10. CV plots and double-layer capacitance of different catalysts. CV plots of a) NP-Ni_{50}, b) NP-$Ni_{25}Cu_{25}$. The CVs were performed at various scan rates (1, 2, 3, 4, and 5 mV s^{-1}) from 0.025 to 0.125 V vs RHE. c) Double-layer capacitance of NP-Ni_{50} and NP-$Ni_{25}Cu_{25}$. d) Catalytic activity is normalized by the electrochemical active surface area (ECSA).

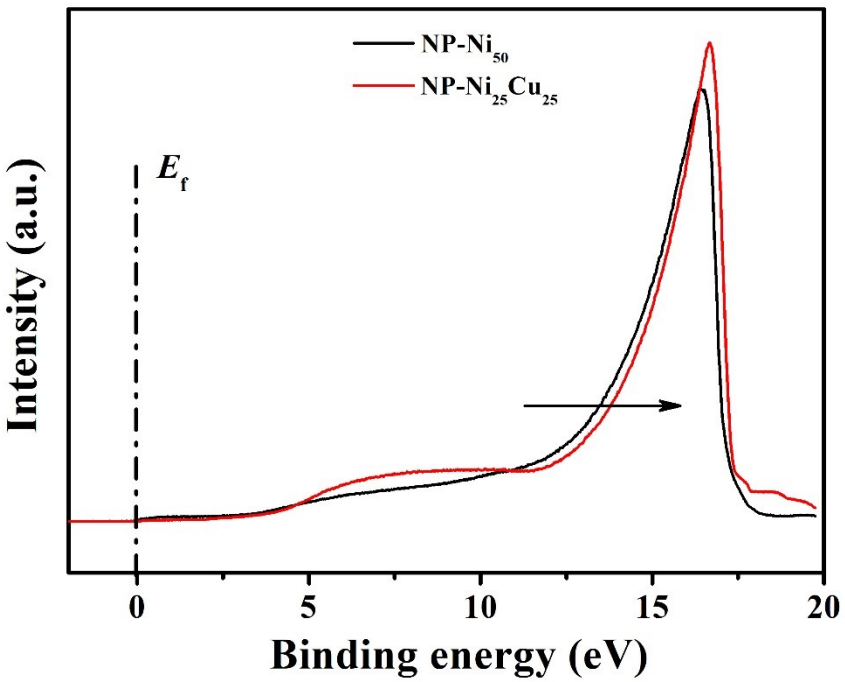

Figure S11. UPS spectra of NP-Ni_{50} (black) and NP-$Ni_{25}Cu_{25}$ (red).

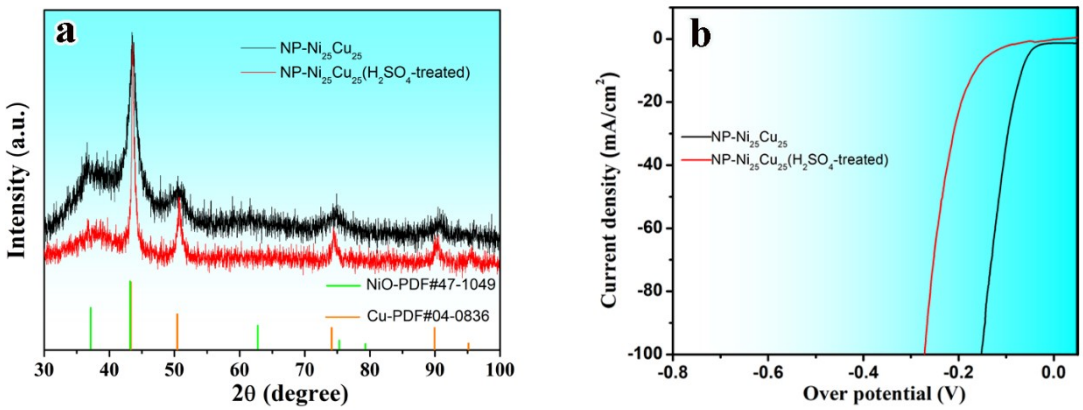

Figure S12. HER activity origin of the NP-$Cu_{25}Ni_{25}$ electrocatalysts. a) XRD patterns of the H_2SO_4 treated NP-$Cu_{25}Ni_{25}$, comparing with the ones of the pristine NP-$Cu_{25}Ni_{25}$. b) HER polarization curves of the H_2SO_4 treated NP-$Cu_{25}Ni_{25}$.

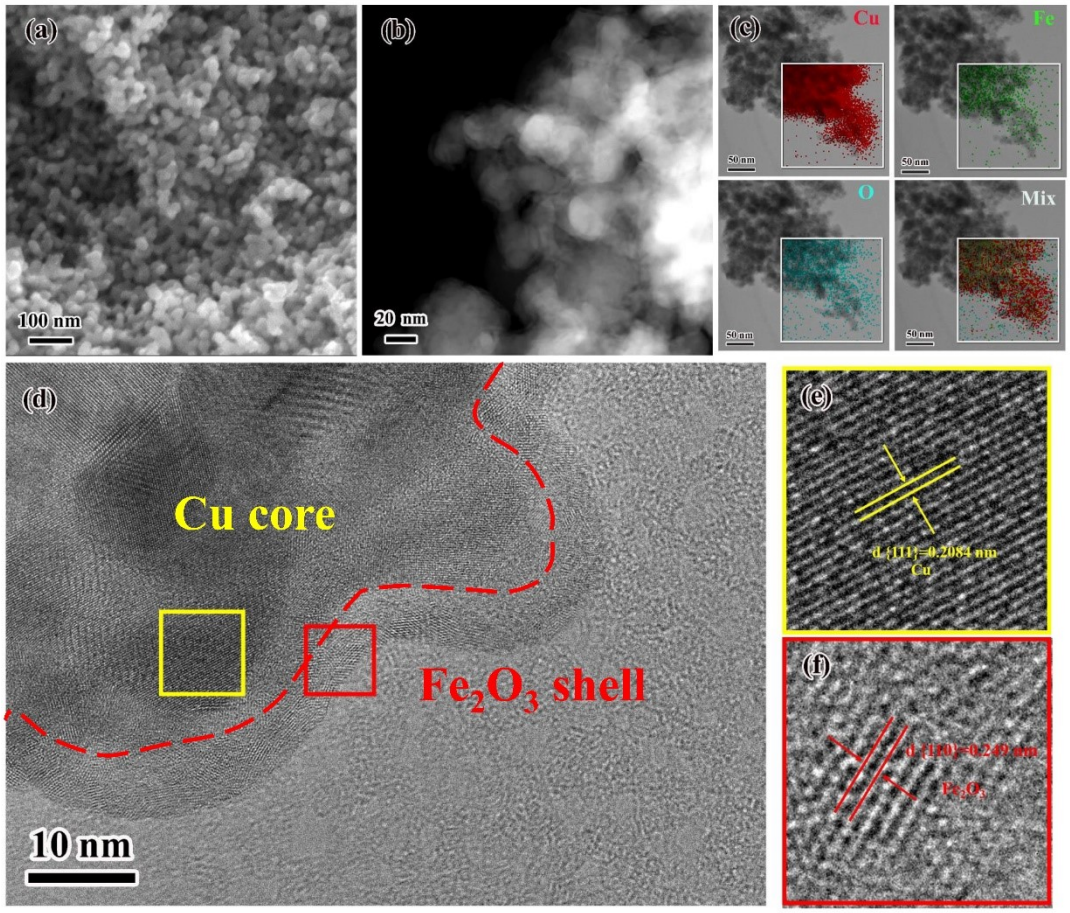

Figure S13. Structural characterizations of the core-shell structured nanoporous Cu@Fe_2O_3/MG. a) SEM micrograph of the dealloyed $Fe_{25}Cu_{25}Zr_{35}Ti_{15}$ MG ribbon. b) and (c) HAADF-STEM and EDS mapping images of NP-$Cu_{25}Fe_{25}$, respectively. d) The HRTEM image of NP-$Cu_{25}Fe_{25}$, and the corresponding HRTEM of (e) the Cu core marked by the yellow square in (d), and f) the Fe_2O_3 shell marked by the red square in (d).

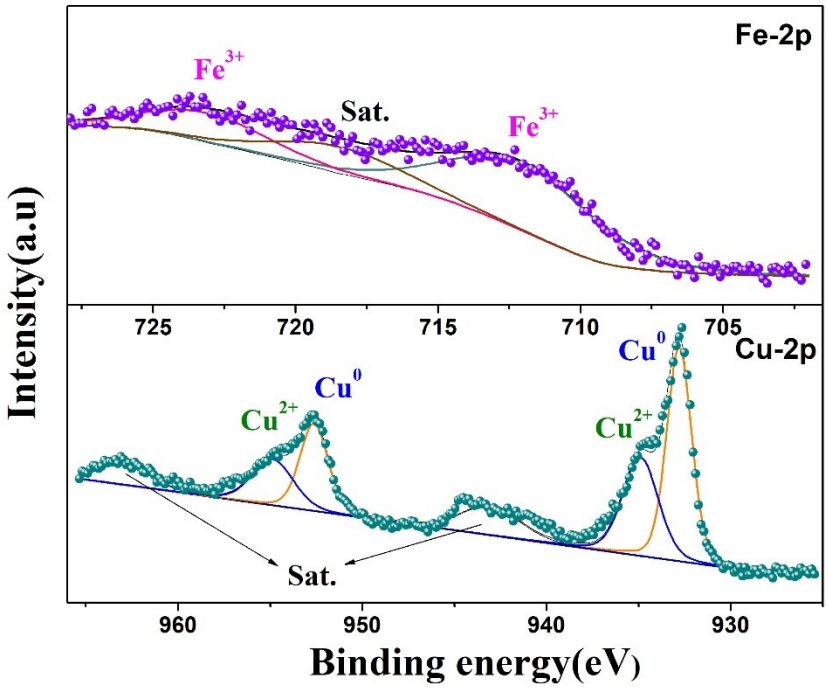

Figure S14. High-resolution XPS spectra of Fe2p and Cu2p of NP- $Fe_{25}Cu_{25}$.

Supplementary Note.

The geometric phase analysis (GPA) technique [5] which was initially proposed for the study of strained metal multilayers and nanocrystals.[6] It has since been applied to a wide variety of systems such as epitaxially grown thin films, quantum dots. [7,8] The accuracy of the technique has been demonstrated by the study of a dislocation in silicon[9].

To do the GPA analyses, a high quality HRTEM image and Digital Micrograph software with the GPA scripts are essential. Firstly, load a HRTEM image into the Digital Micrograph. Then, click on Geometric Phase Analysis, eight additional images and a graphical user interface will appear, and position the circular annotations in the diffractogram to the reflections you want to use for the analysis and press "Read Apertures". Subsequently, need to define an area of perfect (unstrained) crystal by repositioning the region of interest defined in the phase image of refection a*. Finally, output the strain map. For the detailed procedures, please refer to the *Geometric Phase Analysis (GPA) Manual* by C.T. Koch and V.B. Özdöl from the Max Planck Institute for Metals Research for Stuttgart Center for Electron Microscopy.

The HRTEM image was processed by the Digital Micrograph software to produce the GPA diagram, as shown in Fig.2 h, where the compressive strain is represented by the color from green to dark blue, whilst the tensile strain is depicted by the color from red to bright yellow. In our GPA results, dark blue and bright yellow correspond to a fully compressive and tensile strain, respectively, where the color scale limits were set during the Digital Micrograph software processing described above.

As the mechanisms by which compressive and tensile strains improve the HER performance of materials are different, which one contributes primarily to the improvement of the HER performance needs to be analyzed in terms of a case-by-case basis. Specifically, tensile strain lowers the coordination numbers of surface atoms, and thus leads to the reduced bandwidth and an upshifting of *d*-band center. Compressive lattice strain has an opposite effect, resulting in an increased bandwidth and a downshifting of the *d*-band center. Because the antibonding states below the Fermi level are sensitive to *d*-band center position, the above shifting can effectively vary the bindings of adsorbates. The upshifting results in the strengthened bindings with *H intermediates, and vice versa. Thus, if the catalyst is too weak for H intermediates, tensile strain is required to enhance the adsorption of H intermediates; however, if the catalyst is too strong for H intermediates, compressive strain is required to weaken the adsorption of H intermediates. In our case, the catalysts exhibit a weak adsorption of H intermediates. As such, tensile strain plays the dominant contribution for the improved HER performance.

References

[1] M. A. Lukowski, A. S. Daniel, F. Meng, A. Forticaux, L. S. Li, S. Jin, *J. Am. Chem. Soc.*, 2013, **135**, 10274-10277.

[2] M. A. Lukowski, A. S. Daniel, C. R. English, F. Meng, A. Forticaux, R. J. Hamers, S. Jin, *Energy Environ. Sci.*, 2014, **7**, 2608-2613.

[3] *J. Kibsgaard, T. F. Jaramillo, Angew. Chem. Int. Ed.,* 2014, **53**, 14433.

[4] H. L. Fei, J. C. Dong, M. J. Arellano, G. L. Ye, N. D. Kim, E. L. G. Samuel, Z. W. Peng, Z. Zhu, F. Qin, J. M. Bao, M. J. Yacaman, P. M. Ajayan, D. L. Chen, J. M. Tour, *Nat. Commun.,* 2015, **6**, 8668.

[5] M.J. Hy¨tch, E. Snoeck, R. Kilaas, *Ultramicroscopy*, 1998, **74**, 31.

[6] M.J. Hy¨tch, M. Gandais, *Philos. Magn. A*, 1995, **72**, 619.

[7] S. Kret, P. Ruterana, A. Rosenauer, D. Gerthsen, *Phys. Status Solidi (b)*, 2001, **227**, 247.

[8] E. Sarigiannidou, E. Monroy, B. Daudin, J.L. Rouvie`re, A.D. Andreev, *Appl. Phys. Lett.,* 2006, 87, 203112.

[9] M.J. Hy¨tch, J-L. Putaux, J-M. Pe´nisson, *Nature*, 2003, **423**, 270.